Computational Materials Science 245 (2024) 113329

Contents lists available at ScienceDirect

Computational Materials Science

journal homepage: www.elsevier.com/locate/commatsci

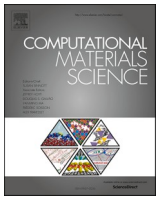

Electronic structure and theoretical exfoliation of non-van der Waals carbonates into low-dimensional materials: A case of $Y_2(CO_3)_3$

Elizaveta A. Kirshneva [a], Lyudmila V. Begunovich [c,d], Dana R. Engelgardt [d,e], Svetlana V. Saikova [b,f], Hans Ågren [g], Artem V. Kuklin [g,*]

[a] School of Petroleum and Natural Gas Engineering, Siberian Federal University, 660041 Krasnoyarsk, Russia
[b] Institute of Chemistry and Chemical Technology, Siberian Branch of the Russian Academy of Sciences, Krasnoyarsk 660036, Russia
[c] Kirensky Institute of Physics, Federal Research Center KSC SB RAS, Akademgorodok, 660036 Krasnoyarsk, Russia
[d] International Research Center of Spectroscopy and Quantu – quantum confiment due m Chemistry - IRC SQC, Siberian Federal University, 660041 Krasnoyarsk, Russia
[e] Department of Chemistry, College of Natural Sciences, Kyungpook National University, 80 Daehak-ro, Buk-gu, Daegu 41566, South Korea
[f] Division of Physical and Inorganic Chemistry, Institute of Non-ferrous Metals, Siberian Federal University, 79 Svobodny pr., 660041 Krasnoyarsk, Russia
[g] Department of Physics and Astronomy, Uppsala University, Box 516, SE-751 20 Uppsala, Sweden

ARTICLE INFO

Keywords:
Yttrium carbonate
Optoelectronic properties
Exfoliation
DFT

ABSTRACT

The unique properties of two-dimensional (2D) materials make them highly versatile for a wide range of applications. Recently, low-dimensional structures obtained from bulk non-van der Waals materials have received particular interest. Yttrium carbonate is an example of such materials which hold the potential for creating 2D structures, however, its fundamental properties have been investigated only rarely. In this work, we demonstrate the possibility of obtaining 2D yttrium carbonate with the tengerite-(Y) structure. The electronic and optical properties of both bulk and two-dimensional $Y_2(CO_3)_3{\cdot}2H_2O$ are investigated using the PBE and HSE06 functionals. While the bulk material is predicted with a bandgap of 7.06 eV at the HSE06 level, the 2D $Y_2(CO_3)_3{\cdot}2H_2O$ material possesses a bandgap of, untypically, 0.4 eV narrower than the bulk material due to surface effects and different stoichiometry. The optical properties reveal that both the bulk and 2D forms are transparent in the visible and near-UV regions positioning them as promising candidates for various optical applications including doping-induced luminescent devices.

1. Introduction

In recent years, 2D materials have gained much attention due to their unique electronic and optical properties, which are significantly different from those of the corresponding bulk materials. This makes it possible to apply such materials in optoelectronics, catalysis, energy storage and generation and sensors, in order to boost the efficiency of devices [1]. Generally, all approaches for the exfoliation of 2D structures can be divided into “top-down” and “bottom-up”. The former includes the well-known scotch-tape method [2,3], micromechanical cleavage and liquid-phase exfoliation. [4], while the latter is typically represented by deposition methods such as chemical and physical vapor deposition (CVD and PVD) [5,6], wet-chemistry synthesis [7,8] and on-surface Ullmann coupling [9,10,11].

A large number of studies on obtaining 2D structures have been carried out for layered van der Waals (vdW) materials, i.e. materials composed of layers where atoms are interconnected by strong chemical bonds while the layers are stacked on each other with van der Waals interactions [2]. Therefore, exfoliation of a single layer of such materials is feasible in many cases and currently the number of exfoliated materials has reached over one hundred, while there are more than one thousand based on theoretical predictions [12]. Such materials include graphite, black phosphorus, transition metal dichalcogenides (TMDs) and others [13,14,3]. TMDs, such as molybdenum disulfide (MoS_2) and tungsten diselenide (WSe_2), exhibit direct bandgaps in the visible range, making them suitable for optoelectronic devices like photodetectors [15,16] and light-emitting diodes (LEDs) [17,18]. Similarly, black phosphorus demonstrates tunable bandgaps and high carrier mobility, offering potential in photovoltaic and photonic applications [19,20].

The production of two-dimensional structures from bulk materials with a covalent bond has recently gained popularity [6,21–23]. Unlike layered materials, which retain their elemental composition, and

* Corresponding author.
E-mail address: artem.kuklin@physics.uu.se (A.V. Kuklin).

https://doi.org/10.1016/j.commatsci.2024.113329
Received 18 July 2023; Received in revised form 23 April 2024; Accepted 24 August 2024
Available online 28 August 2024

stoichiometric ratios after delamination, the delamination of non-vdW materials leads to the formation of two-dimensional materials with a large number of dangling bonds and unsaturated coordination centers caused by the breaking of chemical bonds between the layers [24]. The use of solvents during exfoliation leads to the passivation of the dangling bonds by the formation of new bonds with atoms and functional groups, and the adsorption of solvent molecules on the cleaved surface [25]. This provides an opportunity to modify the surface and obtain functional materials with unique properties suitable for catalysis, spintronics and other fields [26].

The number of experimentally realized non-van der Waals 2D structures grows from year to year. Their most popular representatives include compounds such as hematene [22], ilmenene [27], boron carbide [28,29] and CrTe [30]. Two-dimensional structures based on ilmenite and hematite were among the first to become synthesized. 2D hematite is a semiconductor that exhibits room temperature magnetism and with the potential for various applications in photocatalysis [31]. In addition, Fe_2O_3 can serve as a precursor for the synthesis of low-dimensional structures such as iron phosphide (FeP) [32]. Among p-type semiconductors, low-dimensional B_4C is considered to be one of the most promising materials due to its potential for creating hybrid structures with unique properties, as well as its ability to tune the bandgap width by varying the stoichiometry of boron and carbon [33].

Carbonates of rare earth elements (REEs) are a class of compounds that include carbonate minerals containing a mixture of REEs and synthetic carbonates. The composition of synthetic carbonates of rare earth elements either repeats the composition of the mineral or corresponds to a single-element carbonate without any impurities [34]. These compounds can be used as precursors for the preparation of REE oxides, whose optical, catalytic, and magnetic properties are used in various fields [35]. Synthetic tengerite-Y is an yttrium carbonate with the structural formula $Y_2(CO_3)_3{\cdot}nH_2O$ (n = 2–3). The crystal structure of this material is anisotropic and represented by layers linked to each other by carbonate groups. The properties of this material have rarely been studied and are of interest for future development of carbonates-based materials for various prospective applications [34,36].

In this work, we demonstrate the possibility of 2D phase exfoliation from bulk $Y_2(CO_3)_3{\cdot}2H_2O$. The electronic and optical properties of bulk and 2D $Y_2(CO_3)_3\cdot 2H_2O$ is investigated by using density functional theory. It is predicted that bulk $Y_2(CO_3)_3\cdot 2H_2O$ is a layered non-van der Waals tengerite-Y type material demonstrating a band gap of 5.51 and 7.06 eV at PBE and HSE06 levels of theory, respectively, while 2D yttrium carbonate reveals a band gap narrowing by ~0.4 eV. Optical absorbance spectra indicate prominent absorption in the ultraviolet regions.

The calculations were carried out using the Vienna Ab-initio Simulation Package (VASP) [37,38] applying density functional theory (DFT) and Perdew-Burke-Ernzerhof (PBE) functional [39] corrected by the D3 method proposed by Grimme [40]. To estimate the band gap more accurately, the electronic structure of tengerite-Y was also calculated using the Heyd–Scuseria–Ernzerhof (HSE06) hybrid functional [41]. The cutoff energy of the wave function was chosen as 500 eV. The reciprocal space in the first Brillouin zone was divided into a grid automatically according to the Monkhorst-Pack scheme [42]. The number of k-points for the bulk structure calculation was $9 \times 6 \times 3$, and for the slab models it was $6 \times 4 \times 1$. The convergence tolerances of the force and electronic minimizations were 10^{-2} eV/Å and 10^{-4} eV, respectively. To visualize the atomic structures, the Visualization for Electronic and Structural Analysis (VESTA) software [43] was utilized. The optical properties were calculated time-dependently (TDDFT) within the Tamm–Dancoff approximation by solving the Casida equation [44–46].

The unit cell of bulk $Y_2(CO_3)_3{\cdot}2H_2O$ contains 80 atoms with the structural formula of $Y_8C_{12}O_{44}H_{16}$. The tengerite-Y structure has corrugated layers formed by Y polyhedra in ninefold coordination with the carbonate groups. The layers are bonded to each other by the CO_3 groups [47]. The initial structure was adopted from X-ray diffraction studies by Miyawaki R et al. [48] and then optimized. The minimization of energy results in a slight change in lattice constants (a = 6.02 Å, b = 9.15 Å and c = 15.24 Å) which are in fair agreement with the experimental ones (a = 6.08 Å, b = 9.16 Å and c = 15.10 Å). The unit cell of $Y_2(CO_3)_3{\cdot}2H_2O$ is presented in Fig. 1 (a); the direction of a, b and c corresponds to x, y, z axis respectively. The band structure and density of states (DOS) calculated using the GGA-PBE functional are shown in Fig. 1 (b,c) respectively. The material is found to possess insulating properties with a band gap of 5.51 eV. At the same time, DOS calculated within the HSE06 hybrid functional (Fig. 1(d)) reveals a band gap of 7.06 eV. The valence band maximum (VBM) is located at the YΓ points. However, the FΔ points demonstrate the same energy as the YΓ points and could therefore also be involved in interband transitions. The conduction band minimum (CBM) locates at the YΓ point, revealing a direct band gap type for $Y_2(CO_3)_3{\cdot}2H_2O$. One can also see a high density of states and flat band distribution in the VBM that could refer to heavy holes.

The possibility to produce 2D materials by mechanical exfoliation can be estimated by the cleavage energies of the carbonate and following comparison with the energies of the materials exfoliated experimentally such as alpha-Fe_2O_3 [20] and FeS_2 [21]. To calculate the cleavage energy of yttrium carbonate, a (0 0 1) slab model with a thickness of 47 Å (3 unit cells or 6 layers (two layers are demonstrated in Fig. 1(a)) with a vacuum gap of ~23 Å along the *z* direction was constructed. The cleavage direction was chosen based on the structural anisotropy of the yttrium carbonate crystal and it was assumed that the material can be cleaved along the carbonate groups which link layers between each other. Cleavage leads to two possible surface terminations where the carbonate group can be preserved in the bulk phase or appear in the 2D phase. The schematic representation of exfoliation is shown in Fig. 2 (a). Two layers of yttrium carbonate were constantly separated from the slab at a distance of 1 to 8 Å with a step of 1 Å. We adopted a 2D model where the carbonate group is kept with the bulk part of the slab and therefore does not appear in the considered 2D phase. Then single-point energies were calculated.

Fig. 2(b) shows the dependence of the cleavage energies on the distance between layers for $Y_2(CO_3)_3{\cdot}2H_2O$, Fe_2O_3 и Fe_2S. The cleavage energy (E_{cl}) energy was calculated as:

$$E_{cl} = (E_i - E_0)/S$$

where E_i is the energy of a 2D structure, E_0 is the energy of the bulk, and S is the surface area.

It can be seen that the cleavage energies for pyrite, which has been exfoliated previously, and yttrium carbonate are quite similar to each other and equal to 3.83 J/m^2. At the same time, the cleavage energy of the experimentally realized hematite is higher. This provides some promise that the production of 2D structures of yttrium carbonate can be carried out by liquid-phase exfoliation similar to what has been accomplished for Fe_2O_3 and FeS_2.

We carried out ab-initio molecular dynamic (AIMD) calculations to elucidate stability of the 2D carbonate. The results revieal that part of water molecules can be evaporated from the surface of the carbonate. However, the core structure remains stable.

A bilayer 2D yttrium carbonate (0 0 1) with a vacuum gap of ~15 Å along the *z* direction was then optimized (a = 6.00 Å, b = 9.11 Å) – its structure is presented in Fig. 3(a). The thickness of the 2D slab was 15.63 Å. The stoichiometry in the 2D phase ($Y_8C_{10}O_{46}H_{28}$) is different from that of the bulk ($Y_8C_{12}O_{44}H_{16}$) because there are 92 atoms per unit cell. Transition to the two-layer structure reduces the number of carbon atoms, as interlayer carbonate groups remain attached to the bulk phase during delamination. However, new bonds are formed with OH groups and hydrogen cations at the sites of broken bonds, resulting in an increase in the number of H and O atoms compared to the bulk material. This causes a minor difference in the electronic properties of the

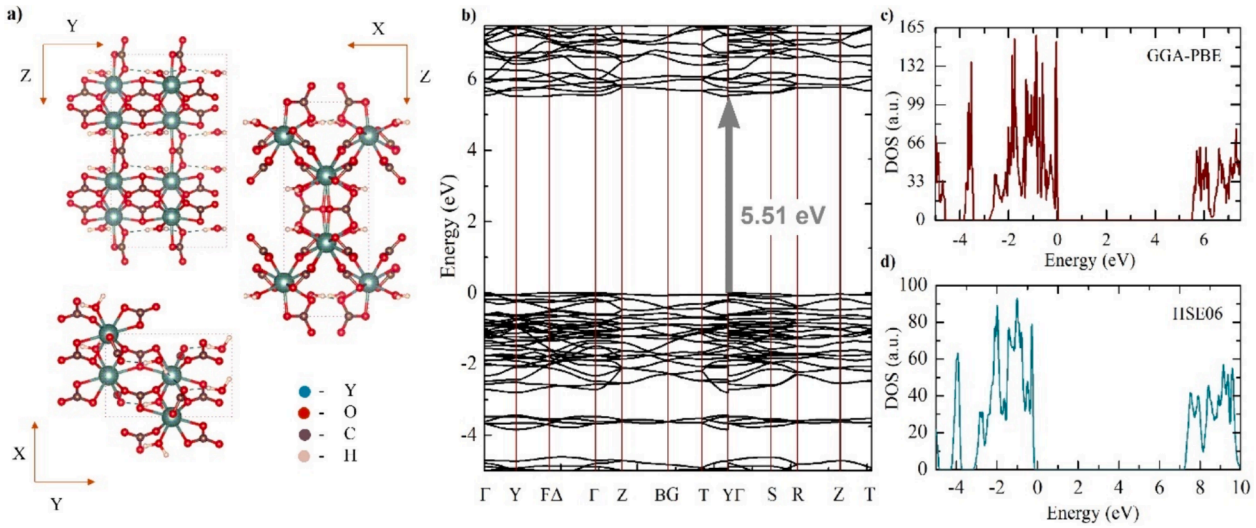

Fig. 1. (a) Atomic structure of $Y_2(CO_3)_3{\cdot}2H_2O$ and its projections on the Y-Z, X-Y and X-Z planes. (b) Band structure of $Y_2(CO_3)_3{\cdot}2H_2O$ calculated at the PBE level. The Fermi level is set to 0 eV. (c, d) Density of states of $Y_2(CO_3)_3{\cdot}2H_2O$ calculated at the PBE (c) and HSE06 (d) levels. The Fermi level is set to 0 eV in both cases.

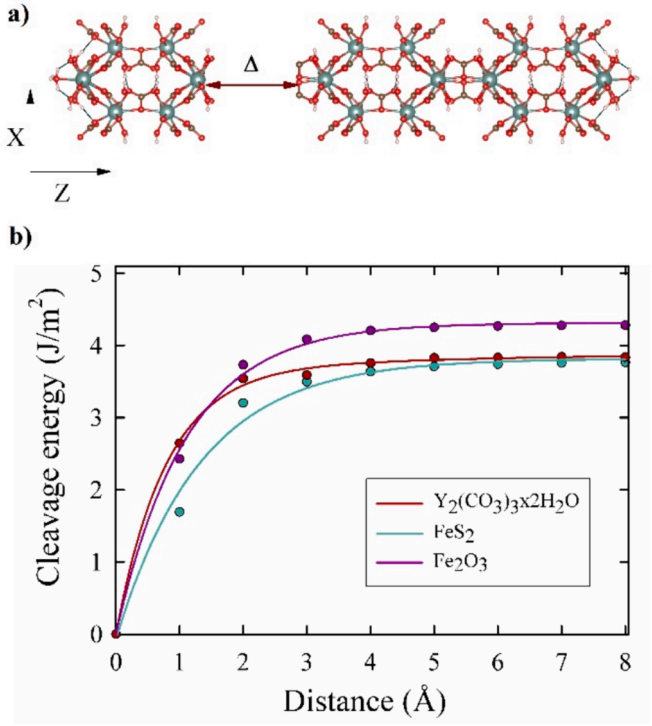

Fig. 2. (a) Representation of tengerite-(Y) exfoliation. (b) Calculated cleavage energies of $Y_2(CO_3)_3{\cdot}2H_2O$, Fe_2O_3 (0 1 0) и FeS_2 (1 1 1).

exfoliated 2D material. Fig. 3(b, c) shows the band structure and DOS of 2D tengerite-(Y) calculated using GGA-PBE. The found band gap is ~0.4 eV narrower as compared to the bulk structure and equals 5.10 eV, also indicating insulating properties. Both VBM and CBM are located at the G-point indicating that the 2D structure of yttrium carbonate, as well as the bulk material, is of a direct band gap type. Densities of states calculated within the HSE06 hybrid functional (Fig. 3(d)) reveal a band gap of 6.75 eV which gives a similar decrease of ~0.4 eV as compared to the bulk. We found that the desorption of two water molecules per unit cell makes only an insignificant effect on the electronic structure. The band distribution is very similar despite the small shift in some energies.

To estimate the transport properties of yttrium carbonate, we determined its electron effective masses in bulk and 2D phases through a second-order polynomial fitting method. Notably, the 2D phase demonstrates the electron effective mass (m*) of 3.29 of the electron rest mass (m_0), which is almost twice better compared to the bulk (7.18 m_0).

At the atomic scale, the transition from bulk yttrium carbonate to 2D structures involves significant surface effects and structural rearrangements. As the material is exfoliated into thinner layers, the surface-to-volume ratio increases, leading to enhanced surface interactions and modified electronic structures. These surface effects can alter the absorption and emission properties of the material by influencing charge carrier dynamics, exciton formation, and photon scattering processes. The transformation from bulk to 2D also introduces changes in stoichiometry in this case. One can see that these deviations from ideal stoichiometry affect the electronic band structure by narrowing the band gap, thereby influencing the material optical properties.

The optical properties presented in Fig. 4 were calculated using the TDDFT method. The results indicate that $Y_2(CO_3)_3{\cdot}2H_2O$ is transparent in the visible and near-ultraviolet range. The bulk material begins to absorb light at 170–180 nm corresponding to its band gap. The absorption reaches a maximum in the UV region of the spectrum at a wavelength of $\lambda = 155$ nm. The 2D yttrium carbonate possesses similar optical properties (Fig. 4b) while its absorption maximum is blue shifted with respect to the bulk and is located at $\lambda = 135$ nm. A following doping strategy, especially with a significant amount of charge carriers, may help to vary the band gap and achieve higher conductivity [49].

While theoretical calculations suggest the feasibility of exfoliating bulk yttrium tengerite (Y) into 2D layers, experimental verification of this process may encounter some challenges. The assumption regarding the possibility of exfoliating bulk yttrium tengerite (Y) into 2D layers is based on the calculation of the crystal cleavage energy. This characteristic depends on the strength of the interatomic bonds within the crystal. However, our model does not account for the interaction of the resulting low-dimensional materials with a solvent. This process generally affects both the stability of 2D structures and the properties of the resulting products, highlighting the importance of selecting an appropriate solvent during experimental work [50]. Furthermore, the ultrasonic treatment of bulk materials has a significant impact on the formation of low-dimensional structures. The processing time and ultrasound frequency exert substantial influence on the size of the final synthesis products [51].

In conclusion, the electronic and optical properties of bulk and two-dimensional (2D) yttrium carbonate were investigated by density functional theory. The results indicate that this material has insulating

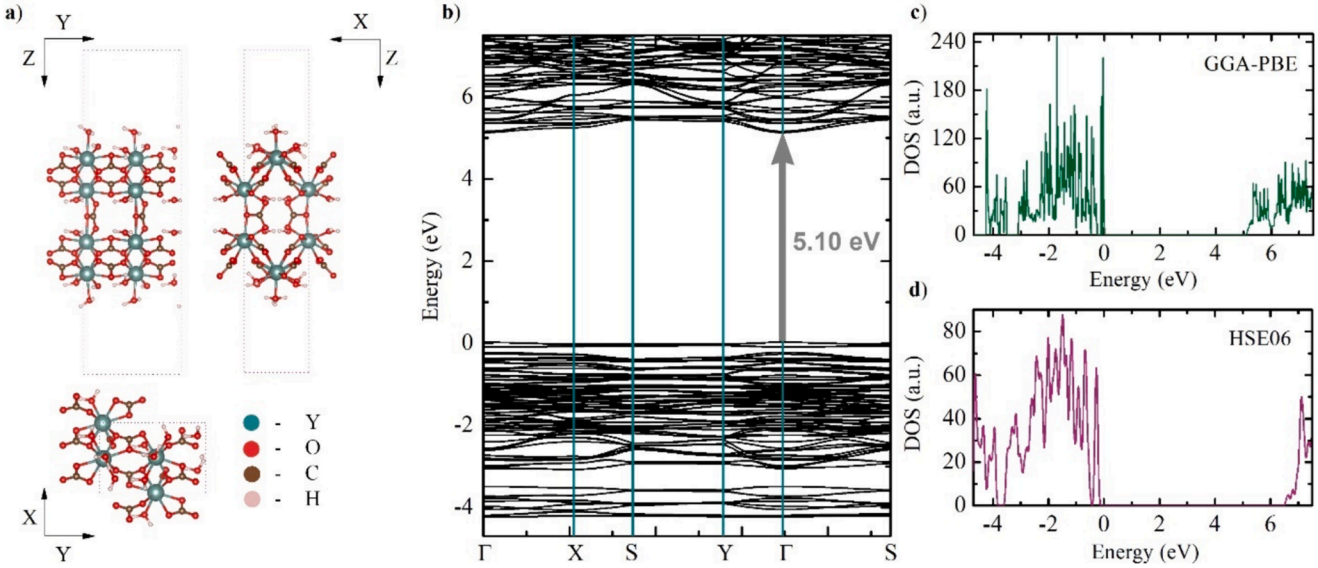

Fig. 3. (a) Atomic structure of two-dimensional $Y_2(CO_3)_3{\cdot}2H_2O$ and its projections on the Y-Z, X-Y and X-Z planes (b) Band structure of 2D $Y_2(CO_3)_3{\cdot}2H_2O$ calculated at the PBE level. The Fermi level is set to 0 eV. (c, d) Density of states of 2D $Y_2(CO_3)_3{\cdot}2H_2O$ calculated at the PBE (c) and HSE06 (d) levels. The Fermi level is set to 0 eV in both cases.

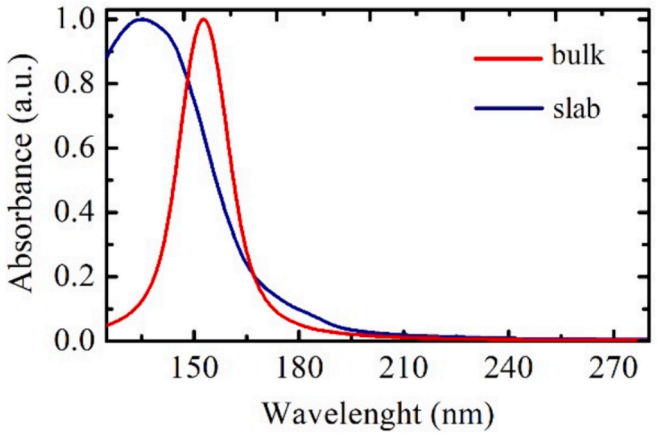

Fig. 4. Optical absorbance curve of bulk (red line) and slab (blue line) $Y_2(CO_3)_3{\cdot}2H_2O$. (For interpretation of the references to colour in this figure legend, the reader is referred to the web version of this article.)

properties and that the transition from bulk to 2D structure is accompanied by a slight decrease in the bandgap of approximately 0.4 eV. An optical property analysis showed that both bulk and 2D $Y_2(CO_3)_3{\cdot}2H_2O$ are transparent in the visible and near-UV regions. Following doping strategy may be applied to make them luminescent material. The calculated exfoliation energy thus suggests that 2D yttrium carbonate has the potential to be obtained using top-down methods, such as liquid phase exfoliation.

CRediT authorship contribution statement

Elizaveta A. Kirshneva: Formal analysis, Investigation, Writing – original draft, Writing – review & editing. **Lyudmila V. Begunovich:** Formal analysis, Writing – review & editing. **Dana R. Engelgardt:** Investigation. **Svetlana V. Saikova:** Conceptualization, Supervision, Writing – review & editing. **Hans Ågren:** Resources, Writing – review & editing. **Artem V. Kuklin:** Conceptualization, Data curation, Formal analysis, Investigation, Software, Supervision, Validation, Writing – original draft, Writing – review & editing.

Declaration of competing interest

The authors declare that they have no known competing financial interests or personal relationships that could have appeared to influence the work reported in this paper.

Data availability

Data will be made available on request.

Acknowledgments

The Russian part of the team acknowledges the support of the Russian Science Foundation (Project 22-73-10047). L.V.B. would like to thank the Information Technology Center, Novosibirsk State University for providing access to supercomputer facilities and the Irkutsk Supercomputer Center of SB RAS for providing access to HPC-cluster «Akademik V.M. Matrosov» (Irkutsk Supercomputer Center of SB RAS). A.K. and H.Å. thank the National Academic Infrastructure for Supercomputing in Sweden (NAISS) and the Swedish National Infrastructure for Computing (SNIC) at the National Supercomputer Centre of Linköping University partially funded by the Swedish Research Council through grant agreements no. 2022-06725 and no. 2018-05973.

References

[1] R. Dong, T. Zhang, X. Feng, Interface-assisted synthesis of 2D materials: trend and challenges, Chem. Rev. 118 (2018) 6189, https://doi.org/10.1021/acs.chemrev.8b00056.
[2] C. Tan, X. Cao, X.J. Wu, Q. He, J. Yang, X. Zhang, J. Chen, W. Zhao, S. Han, G. H. Nam, et al., Recent advances in ultrathin two-dimensional nanomaterials, Chem. Rev. 117 (9) (2017) 6225, https://doi.org/10.1021/acs.chemrev.6b00558.
[3] K.S. Novoselov, A.K. Geim, S.V. Morozov, D.E. Jiang, Y. Zhang, S.V. Dubonos, I. V. Grigorieva, A.A. Firsov, Electric field effect in atomically thin carbon films, Science 306, 666 (2004), Science 306 (2004) 666–669, https://doi.org/10.1126/science.1102896.
[4] M. Yi, Z. Shen, A review on mechanical exfoliation for the scalable production of graphene, J. Mater. Chem. A 3 (2015) 11700, https://doi.org/10.1039/C5TA00252D.
[5] K.K. Kim, A. Hsu, X. Jia, S.M. Kim, Y. Shi, M. Hofmann, D. Nezich, J.F. Rodriguez-Nieva, M. Dresselhaus, T. Palacios, et al., Synthesis of monolayer hexagonal boron nitride on Cu foil using chemical vapor deposition, Nano Lett. 12 (2012) 161, https://doi.org/10.1021/nl203249a.

[6] J. Yuan, A. Balk, H. Guo, Q. Fang, S. Patel, X. Zhao, T. Terlier, D. Natelson, S. Crooker, J. Lou, Room-temperature magnetic order in air-stable ultrathin iron oxide, Nano Lett. 19 (2019) 3777, https://doi.org/10.1021/acs.nanolett.9b00905.

[7] M.S. Pawar, D.J. Late, Temperature-dependent Raman spectroscopy and sensor applications of PtSe2 nanosheets synthesized by wet chemistry, Beilstein J. Nanotechnol. 10 (2019) 467, https://doi.org/10.3762/bjnano.10.46.

[8] C. Altavilla, M. Sarno, P. Ciambelli, A novel wet chemistry approach for the synthesis of hybrid 2D free-floating single or multilayer nanosheets of MS2@ oleylamine (M=Mo, W), Chem. Mater. 23 (2011) 3879, https://doi.org/10.1021/cm200837g.

[9] T.A. Pham, F. Song, M.T. Nguyen, Z. Li, F. Studener, M. Stöhr, Comparing Ullmann coupling on noble metal surfaces: on-surface polymerization of 1, 3, 6, 8-tetra-bromopyrene on Cu (111) and Au (111), Chem. Eur. J. 22 (2016) 5937, https://doi.org/10.1002/chem.201504946.

[10] J. Rodríguez-Fernández, M.J. Haastrup, S.B. Schmidt, S.S. Grønborg, M. H. Mammen, J.V. Lauritsen, Molecular nanowire bonding to epitaxial single-layer MoS2 by an on-surface ullmann coupling reaction, Small 16 (2020) 1906892, https://doi.org/10.1002/smll.201906892.

[11] X. Xu, T. Guo, H. Kim, M.K. Hota, R.S. Alsaadi, M. Lanza, X. Zhang, H.N. Alshareef, Growth of 2D materials at the wafer scale, Adv. Mater. 34 (2022) 2108258, https://doi.org/10.1002/adma.202108258.

[12] K. Choudhary, K.F. Garrity, S.T. Hartman, G. Pilania, F. Tavazza, Efficient computational design of two-dimensional van der Waals heterostructures: Band alignment, lattice mismatch, and machine learning, Phys. Rev. Mater. 7 (2023) 014009, https://doi.org/10.1103/PhysRevMaterials.7.014009.

[13] H. Li, J. Wu, Z. Yin, H. Zhang, Preparation and applications of mechanically exfoliated single-layer and multilayer MoS2 and WSe2 nanosheets, Acc. Chem. Res. 47 (2014) 1067, https://doi.org/10.1021/ar4002312.

[14] J.N. Coleman, M. Lotya, A. O'Neill, S.D. Bergin, P.J. King, U. Khan, K. Young, A. Gaucher, S. De, R.J. Smith, et al., Two-dimensional nanosheets produced by liquid exfoliation of layered materials, Science 331 (2011) 568, https://doi.org/10.1126/science.119497.

[15] H. Qiao, Z. Huang, X. Ren, S. Liu, Y. Zhang, X. Qi, H. Zhang, Self-powered photodetectors based on 2D materials, Adv. Opt. Mater. 8 (2020) 1900765, https://doi.org/10.1002/ADOM.201900765.

[16] A. Taffelli, S. Dirè, A. Quaranta, L. Pancheri, MoS2 based photodetectors: a review, Sensors 21 (2021) 2758, https://doi.org/10.3390/S21082758.

[17] S. Hwangbo, L. Hu, A.T. Hoang, J.Y. Choi, J.H. Ahn, Wafer-scale monolithic integration of full-colour micro-LED display using MoS2 transistor, Nat. Nanotechnol. 175 (17) (2022) 500–506, https://doi.org/10.1038/s41565-022-01102-7.

[18] C. Wang, F. Yang, Y. Gao, The highly-efficient light-emitting diodes based on transition metal dichalcogenides: from architecture to performance, Nanoscale Adv. 2 (2020) 4323–4340, https://doi.org/10.1039/D0NA00501K.

[19] X. Wang, S. Lan, Optical properties of black phosphorus, Adv. Opt. Photonics 8 (2016) 618–655, https://doi.org/10.1364/AOP.8.000618.

[20] B. Guo, Q. Lan Xiao, S. Hao Wang, H. Zhang, 2D layered materials: synthesis, nonlinear optical properties, and device applications, laser photon, Rev. 13 (2019) 1800327, https://doi.org/10.1002/LPOR.201800327.

[21] T.P. Yadav, S.N. Shirodkar, N. Lertcumfu, S. Radhakrishnan, F.N. Sayed, K. D. Malviya, G. Costin, R. Vajtai, B.I. Yakobson, C.S. Tiwary, et al., Chromiteen: a new 2D oxide magnetic material from natural ore, Adv. Mater. Interfaces 5 (2018) 1800549, https://doi.org/10.1002/admi.201800549.

[22] A. Puthirath Balan, S. Radhakrishnan, C.F. Woellner, S.K. Sinha, L. Deng, C.D. L. Reyes, B.M. Rao, M. Paulose, R. Neupane, A. Apte, et al., Exfoliation of a non-van der Waals material from iron ore hematite, Nat. Nanotechnol. 13 (2018) 602, https://doi.org/10.1038/s41565-018-0134-y.

[23] A.B. Puthirath, A.P. Balan, E.F. Oliveira, V. Sreepal, F.C. Robles Hernandez, G. Gao, N. Chakingal, L.M. Sassi, P. Thibeorchews, G. Costin, et al., Apparent ferromagnetism in exfoliated ultrathin pyrite sheets, J. Phys. Chem. C 125 (2021) 18927, https://doi.org/10.1021/acs.jpcc.1c04977.

[24] C. Jin, L. Kou, Two-dimensional non-van der Waals magnetic layers: functional materials for potential device applications, J. Phys. d: Appl. Phys. 54 (2021) 413001, https://doi.org/10.1088/1361-6463/ac08ca.

[25] Y. Wei, M. Ghorbani-Asl, A.V. Krasheninnikov, Tailoring the electronic and magnetic properties of hematene by surface passivation: insights from first-principles calculations, J. Phys. Chem. C 124 (2020) 22784, https://doi.org/10.1021/acs.jpcc.0c05807.

[26] I. Tantis, S. Talande, V. Tzitzios, G. Basina, V. Shrivastav, A. Bakandritsos, R. Zboril, Non-van der Waals 2D materials for electrochemical energy storage, Adv. Funct. Mater. 33 (2023) 2209360, https://doi.org/10.1002/adfm.202209360.

[27] A. Puthirath Balan, S. Radhakrishnan, R. Kumar, R. Neupane, S.K. Sinha, L. Deng, C.A.D.L. Reyes, A. Apte, B. Manmadha Rao, M. Paulose, et al., A non-van der Waals two-dimensional material from natural titanium mineral ore ilmenite, Chem. Mater. 30 (2018) 5923, https://doi.org/10.1021/acs.chemmater.8b01935.

[28] R.F. Gunnewiek, P.M. Souto, R.H. Kiminami, Synthesis of nanocrystalline boron carbide by direct microwave carbothermal reduction of boric acid, J. Nanomater. 2017 (2017) 3983468, https://doi.org/10.1155/2017/3983468.

[29] M. Kakiage, N. Tahara, S. Yanagidani, I. Yanase, H. Kobayashi, Effect of boron oxide/carbon arrangement of precursor derived from condensed polymer-boric acid product on low-temperature synthesis of boron carbide powder, J. Ceram. Soc. Jpn. 119 (2011) 422, https://doi.org/10.2109/jcersj2.119.422.

[30] M. Wang, L. Kang, J. Su, L. Zhang, H. Dai, H. Cheng, X. Han, T. Zhai, Z. Liu, J. Han, Two-dimensional ferromagnetism in CrTe flakes down to atomically thin layers, Nanoscale 12 (2020) 16427, https://doi.org/10.1039/D0NR04108D.

[31] Y. Su, H. Wang, S. Wang, L. Hao, B. Fang, M. Wan, Q. Chen, K. He, J. Zhang, Q. Wang, The electronic, optical and water splitting properties in two-dimensional hematite Fe2O3 semiconductors with uniaxial, biaxial strain studied by first principles, Phys. E: Low-Dimens. Syst. Nanostruct. 149 (2023) 115667, https://doi.org/10.1016/j.physe.2023.115667.

[32] M. Mohiuddin, A. Zavabeti, F. Haque, A. Mahmood, R.S. Datta, N. Syed, M. W. Khan, A. Jannat, K. Messalea, B.Y. Zhang, et al., Synthesis of two-dimensional hematite and iron phosphide for hydrogen evolution, J. Mater. Chem. A 8 (2020) 2789, https://doi.org/10.1039/C9TA11945K.

[33] L. Zhou, J. Gao, Y. Liu, J. Liang, M. Javid, A. Shah, X. Dong, H. Yu, X. Quan, Template synthesis of novel monolayer B4C ultrathin film, Ceram. Int. 45 (2019) 2909, https://doi.org/10.1016/j.ceramint.2018.10.216.

[34] P. Kim, A. Anderko, A. Navrotsky, R.E. Riman, Trends in structure and thermodynamic properties of normal rare earth carbonates and rare earth hydroxycarbonates, Minerals 8 (2018) 106, https://doi.org/10.3390/min8030106.

[35] Y. Zhang, M. Gao, K. Han, Z. Fang, X. Yin, Z. Xu, Synthesis, characterization and formation mechanism of dumbbell-like YOHCO3 and rod-like Y2 (CO3) 3· 2.5 H2O, J. Alloy. Compd. 474 (2009) 598, doi: 10.1016/j.jallcom.2008.07.007.

[36] A.M. Kaczmarek, K. Van Hecke, R. Van Deun, Nano-and micro-sized rare-earth carbonates and their use as precursors and sacrificial templates for the synthesis of new innovative materials, Chem. Soc. Rev. 44 (2015) 2032, https://doi.org/10.1039/C4CS00433G.

[37] G. Kresse, J. Furthmüller, Efficient iterative schemes for ab initio total-energy calculations using a plane-wave basis set, Phys. Rev. B 54 (1996) 11169, https://doi.org/10.1103/PhysRevB.54.11169.

[38] G. Kresse, J. Hafner, Ab initio molecular dynamics for liquid metals, Phys. Rev. B 47 (1993) 558, https://doi.org/10.1103/PhysRevB.47.558.

[39] J.P. Perdew, K. Burke, M. Ernzerhof, Generalized gradient approximation made simple, Phys. Rev. Lett. 77 (1996) 3865, https://doi.org/10.1103/PhysRevLett.77.3865.

[40] S. Grimme, J. Antony, S. Ehrlich, H. Krieg, A consistent and accurate ab initio parametrization of density functional dispersion correction (DFT-D) for the 94 elements H-Pu, J. Chem. Phys. 132 (2010) 154104, https://doi.org/10.1063/1.3382344.

[41] J. Heyd, G.E. Scuseria, M. Ernzerhof, Hybrid functionals based on a screened Coulomb potential, J. Chem. Phys. 118 (2003) 8207, https://doi.org/10.1063/1.1564060.

[42] H.J. Monkhorst, J.D. Pack, Special points for Brillouin-zone integrations, Phys. Rev. B 13 (1976) 5188, https://doi.org/10.1103/PhysRevB.13.5188.

[43] K. Momma, F. Izumi, VESTA 3 for three-dimensional visualization of crystal, volumetric and morphology data, J. Appl. Cryst. 44 (2011) 1272, https://doi.org/10.1107/S0021889811038970.

[44] L.X. Benedict, E.L. Shirley, R.B. Bohn, Optical absorption of insulators and the electron-hole interaction: an ab initio calculation, Phys. Rev. Lett. 80 (1998) 4514, https://doi.org/10.1103/PhysRevLett.80.4514.

[45] S. Albrecht, L. Reining, R. Del Sole, G. Onida, Ab initio calculation of excitonic effects in the optical spectra of semiconductors, Phys. Rev. Lett. 80 (1998) 4510, https://doi.org/10.1103/PhysRevLett.80.4510.

[46] M. Rohlfing, S.G. Louie, Electron-hole excitations in semiconductors and insulators, Phys. Rev. Lett. 81 (1998) 2312, https://doi.org/10.1103/PhysRevLett.81.2312.

[47] A.V. Voloshin, Experience in taxonomy of Y and REE carbonates, Bull. Murmansk State Tech. Univ. 3 (2000) 245.

[48] R. Miyawaki, S. Matsubara, A refinement of the crystal structure of synthetic tengerite-(Y), Bull. Natn. Sci. Mus. Ser. C 30 (2004) 1.

[49] A. Paulraj, P. Natarajan, K. Munnisamy, M.K. Nagoor, K. Parimana Nattar, B. Abdulrazak, J. Duraisamy, Photoluminescence efficiencies of nanocrystalline versus bulk Y2O3: Eu phosphor—revisited, J. Am. Ceram. Soc. 94 (2011) 1627, https://doi.org/10.1111/j.1551-2916.2010.04246.x.

[50] M. Telkhozhayeva, E. Teblum, R. Konar, O. Girshevitz, I. Perelshtein, H. Aviv, Y. R. Tischler, G.D. Nessim, Higher ultrasonic frequency liquid phase exfoliation leads to larger and monolayer to few-layer flakes of 2D layered materials, Langmuir 37 (2021) 4504–4514, https://doi.org/10.1021/ACS.LANGMUIR.0C03668.

[51] R. Tian, J.N. Coleman, H. Kaur, A. Roy, M. McCrystall, D.V. Horvath, G.L. Onrubia, R. Smith, M. Ruether, A. Griffin, C. Backes, V. Nicolosi, Production of quasi-2d platelets of nonlayered iron pyrite (FeS2) by liquid-phase exfoliation for high performance battery electrodes, ACS Nano. 14 (2020) 13418–13432, https://doi.org/10.1021/ACSNANO.0C05292.